

Wide-blocky veins explained by dependency of crystal growth rate on fracture surface type: Insights from phase-field modeling

Liene Spruženiece¹, Michael Späth², Janos L. Urai¹, Estibalitz Ukar³, Michael Selzer^{2,4} and Britta Nestler^{2,4}

¹Institute of Structural Geology, Tectonics and Geomechanics, RWTH Aachen University, Lochnerstraße 4-20, 52056 Aachen, Germany

²Institute for Applied Materials—Computational Materials Science, Karlsruhe Institute of Technology, Straße am Forum 7, 76131 Karlsruhe, Germany

³Bureau of Economic Geology, Jackson School of Geosciences, The University of Texas at Austin, 10100 Burnet Road, Austin, Texas 78758, USA

⁴Institute of Digital Materials Science, Karlsruhe University of Applied Sciences, Moltkestraße 30, 76133 Karlsruhe, Germany

ABSTRACT

Vein microstructures contain a wealth of information on coupled chemical and mechanical processes of fracturing, fluid transport, and crystal growth. Numerical simulations have been used for exploring the factors controlling the development of vein microstructures; however, they have not been quantitatively validated against natural veins. Here we combined phase-field modeling with microtextural analysis of previously unexplained wide-blocky calcite veins in natural limestone and of the fresh fracture surface in this limestone. Results show that the wide-blocky vein textures can only be reproduced if ~10%–20% of crystals grow faster than the rest. This fraction corresponds to the amount of transgranularly broken grains that were observed on the experimental fracture surfaces, which are dominantly intergranular. We hypothesize that transgranular fractures allow faster growth of vein minerals due to the lack of clay coatings and other nucleation discontinuities that are common along intergranular cracks. Our simulation results show remarkable similarity to the natural veins and reproduce the nonlinear relationship between vein crystal width and vein aperture. This allows accurate simulations of crystal growth processes and related permeability evolution in fractured rocks.

INTRODUCTION

Fractures provide important pathways for fluid migration in Earth's crust (Newhouse, 1942; Cox et al., 1987; Nelson, 2001). Microstructures of minerals precipitated in veins contain a wealth of information on the mechanical, chemical, and hydrothermal history of veins (e.g., Boullier and Robert, 1992; Bons et al., 2012; Ukar and Laubach, 2016; Laubach et al., 2019).

A number of different approaches have been presented for simulating crystal growth kinematics in veins. Early models used geometric projections for exploring kinematics of polycrystals growing in a confined space (Urai et al., 1991; Dickson, 1993) to explain fibrous and elongate-blocky crystal growth. Subsequent numerical methods including front-tracking algorithms of

the Elle numerical simulation platform ([www.http://elle.ws/](http://elle.ws/); Bons, 2001; Hilgers et al., 2001; Nollet et al., 2005) and cellular automation-type models (Lander et al., 2008; Lander and Laubach, 2015) explored anisotropic crystal growth in antitaxial veins, where crystals can develop facets during epitaxial growth from a rough surface toward the inert vein wall. However, the vast majority of veins in rocks at depths of 1–10 km and at 100–350 °C are syntaxial: crystals grow on both fracture sides (Durney and Ramsay, 1973; Bons et al., 2012). More recently, phase-field models were introduced to model both syntaxial and antitaxial veins. Due to the different approach to moving boundaries, these models are more efficient, allowing simulations against dynamic, moving interfaces as crystals

from both sides seal a syntaxial vein, and enabling three-dimensional (3-D) modeling (e.g., Ankit et al., 2015; Wendler et al., 2016; Kling et al., 2017; Prajapati et al., 2020). However, up to now, the phase-field models have not been quantitatively compared with natural vein microstructures.

This study fills this gap by applying the phase-field method to simulate enigmatic wide-blocky microstructures in natural calcite veins from Somerset, UK. We were able to replicate the natural microstructures quantitatively and provide new insights on vein formation mechanisms, showing how variations in transgranular and intergranular segments on fracture surfaces lead to heterogeneous crystal growth, producing microstructures that are not predicted by previous models.

SAMPLES AND METHODS

We analyzed arrays of calcite microveins in Liassic (Lower Jurassic) limestones near Blue Anchor, Kilve, and Lilstock beaches in Somerset, UK (Figs. 1A and 1B). The veins are normal to bedding in the damage zone of regional normal faults (Caputo and Hancock, 1999; Nixon et al., 2019). Double-polished thin sections, cut perpendicular to the veins, were imaged and studied in the PetroScan Virtual Microscope (see Item S1 in the Supplemental Material¹) as well as by scanning electron microscope (SEM)-based cathodoluminescence (CL), secondary electron (SE), and backscattered electron (BSE) imaging (Item S1).

¹Supplemental Material. Analytical methods, description of numerical approach, image library of results, and video files of the 2-D and 3-D simulations. Please visit <https://doi.org/10.1130/GEOL.S.13584911> to access the supplemental material, and contact editing@geosociety.org with any questions.

CITATION: Spruženiece, L., et al., 2021, Wide-blocky veins explained by dependency of crystal growth rate on fracture surface type: Insights from phase-field modeling: *Geology*, v. 49, p. 641–646, <https://doi.org/10.1130/G48472.1>

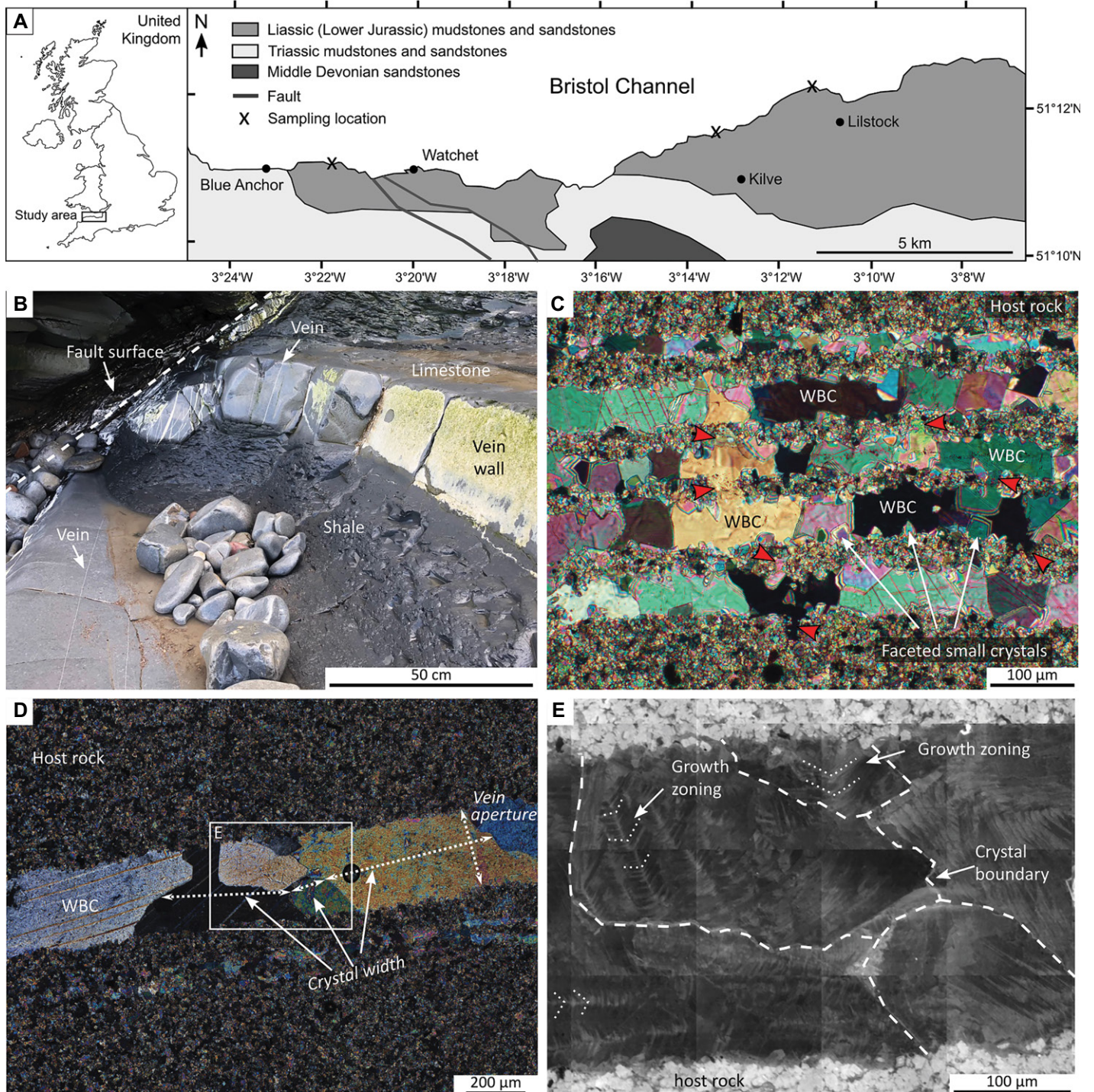


Figure 1. (A) Geologic setting and sampling locations in Somerset, UK (map adapted from Glen et al. [2005] and Peacock and Sanderson [2018]). (B) Outcrop-scale relationships between veins and Liassic (Lower Jurassic) limestone and shale beds. (C,D) Optical micrographs under crossed polarizers showing wide-blocky microstructures. WBC—wide-blocky crystal; red arrows mark host-rock grains in optical continuity with vein crystals. (E) Scanning electron microscope-based cathodoluminescence image showing faceted growth zoning within wide-blocky crystals.

Analysis of fresh fracture surface was performed on $4.5 \times 2 \times 1$ cm blocks of the same rocks broken by three-point loading to obtain mode I fractures parallel to existing veins. Fracture surfaces were imaged in SEM-SE, and transgranular fractures in these images were quantified using Fiji software (Schindelin et al., 2012).

Phase-field vein growth simulations in two and three dimensions (2-D and 3-D) were performed using a multiphase-field approach (e.g., Nestler et al., 2005) (Items S2–S4). Computational fluid dynamics analysis of 3-D microstructure was used to solve fluid flow and permeability changes during the sealing process of the fracture (e.g., Kling et al., 2017).

MICROSTRUCTURAL RESULTS

The host rock is a micritic limestone with $\sim 95\%$ calcite grains, carbonate fossils, and $\sim 5\%$ accessory minerals (quartz, dolomite, albite, clays, and pyrite) (Figs. 1C, 1D, and 2A). It contains sets of subparallel calcite veins with apertures from a few micrometers to several centimeters. The veins that are wider than

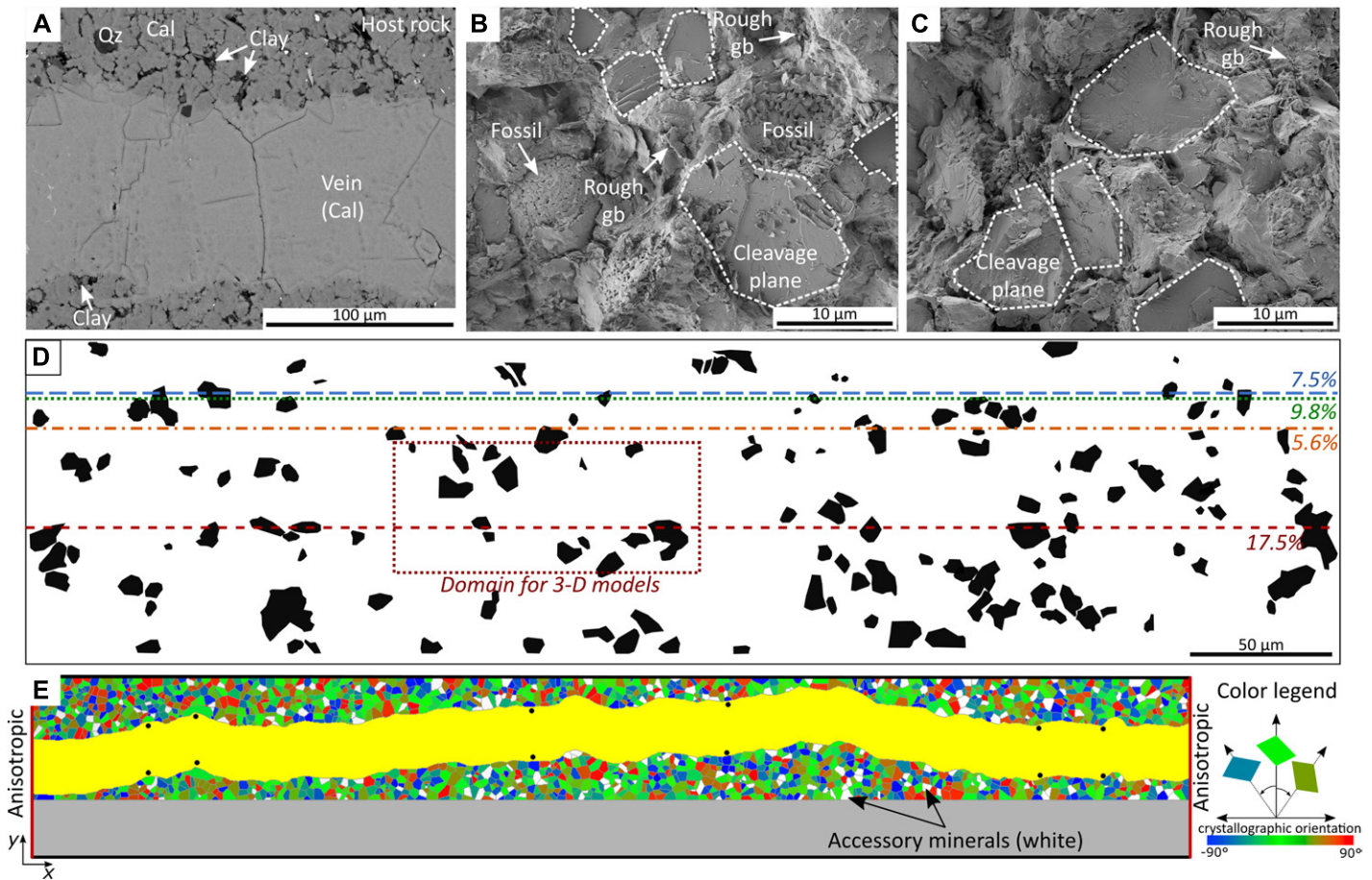


Figure 2. (A) Backscattered electron image of sample cut perpendicular to the vein (Qz—quartz; Cal—calcite). (B,C) Secondary electron images of experimentally broken samples, looking at the fracture surfaces (gb—grain boundary). (D) Distribution of calcite cleavage planes (black; transgranular fractures) on an experimental fracture surface. Four profile lines were used for two-dimensional simulations in Figure 3A, where percentages refer to the proportion of transgranular segments on each profile (see details in Item S2 [see footnote 1]). Rectangle marks the location of the chosen domain for the three-dimensional (3-D) models in Figure 4. (E) Setup for phase-field simulations along the 17.5% profile line in D. “Broken” grains are mirrored and marked with black dots. Color scale shows crystal orientations with respect to the fracture orientation.

1 mm show elongate-blocky microstructures (Fisher and Brantley, 1992; Bons, 2001) with solid inclusion bands suggesting crack-seal processes and growth competition. We focused on microveins (aperture <1 mm) filled by laterally wide, blocky crystals whose formation mechanism remains unexplained (Figs. 1C and 1D). These microveins lack host-rock inclusion bands, suggesting a single crack-seal cycle (Ramsay, 1980). The vein crystals show optical continuity with adjacent grains in the host rock. Smaller equidimensional crystals with euhedral terminations occur along the vein walls, indicating syntaxial growth into an open fracture. SEM-CL images show growth zoning within both small and large crystals, indicating faceted growth toward the vein interior (Figs. 1D and 1E).

A characteristic feature of the 59 analyzed microveins is the relationship between microvein aperture (D_m) and the average width of the crystals (W) as measured along the median line of the vein (Figs. 1D and 3A; Fig. S1 in the Supplemental Material). Both parameters are non-dimensional, scaled against the average

grain diameter in the host rock, so that natural microstructures can be compared with simulated ones. In the narrowest veins, W and D_m are similar: the vein crystal width increases linearly with the increase of the vein aperture (Fig. 3A). For wider veins with $D_m > \sim 4$, W/D_m slowly increases toward 2. At $D_m > \sim 10$, W becomes independent of D_m . For $D_m < \sim 4$, vein crystals are mostly equant, while for $D_m > 4$, they can reach aspect ratios of 10.

Experimental fracture surfaces consist mostly of intergranular, rather than transgranular, segments that follow nano-porous fossil, micritic grain, and accessory mineral boundaries, as recognized in SE images by their surface morphologies (Figs. 2B and 2C). In most cases, such grain boundaries show clay-mineral coatings on calcite. Only $\sim 10\%$ of the fracture surface is transgranular, exposing clean calcite cleavage planes (Fig. 2D).

SETUP OF THE PHASE-FIELD MODEL

Based on our microstructural observations, we hypothesized that precipitation of vein calcite is faster on clean, transgranular microcracks

formed along cleavage planes in the host-rock calcite, and slower on intergranular cracks that are coated by clay minerals (Lander et al., 2008; Ajdukiewicz and Larese, 2012; Williams et al., 2015). The host rock in the 2-D models was generated with a Voronoi algorithm (Fig. 2E; Item S2), where grains have random crystallographic orientations to mimic micrite. The starting fracture shape was based on the geometry of one of the natural veins, with normalized apertures (D_m) varied from 1 to 16 in different simulations. Vein crystals were set to grow epitaxially on host-rock grains into the open fractures, as inferred from microstructures in the natural veins (Figs. 1C and 1E). Crystals were assigned anisotropic surface energy so they could develop facets and vertices corresponding with calcite crystal symmetry. The relative growth rate differences for different fracture surfaces were incorporated as a dimensionless factor ξ . Three types of surfaces were distinguished based on the analysis of natural samples and experimental fracture surfaces (Figs. 2A–2E; Table S3): (1) inert accessory minerals with no epitaxial calcite growth

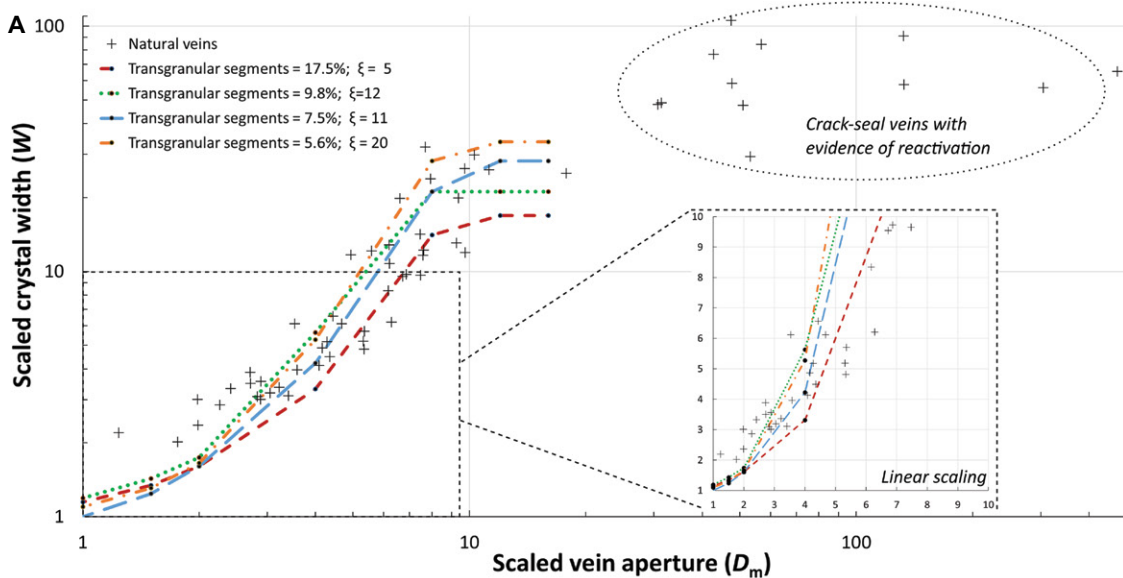
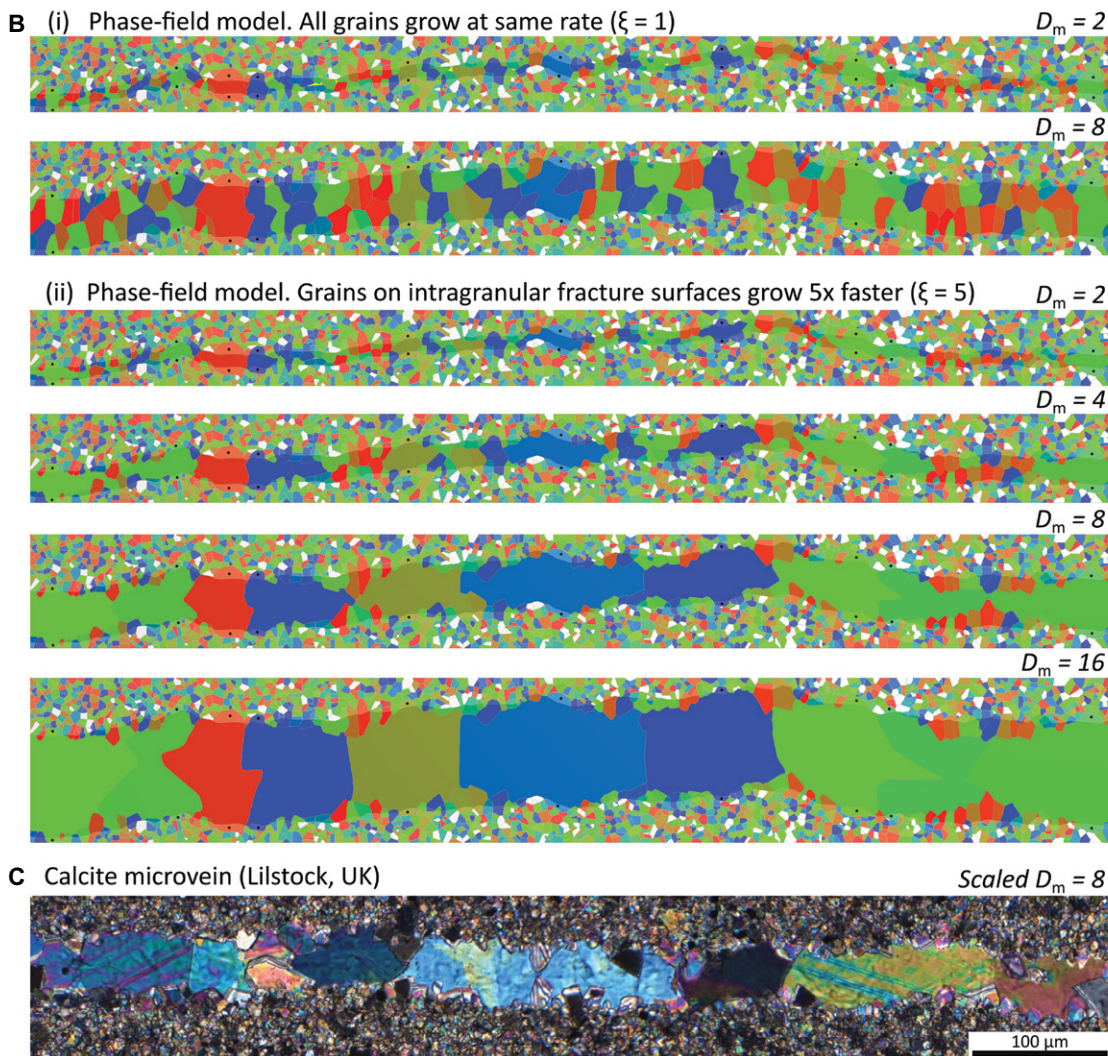


Figure 3. (A) Relationship between vein aperture (D_m) and crystal width (W) in wide-blocky veins from the Somerset, UK, area and simulations (scaled against the average diameter of host-rock grains). Note that the entire data set is scaled logarithmically; in addition, the inset shows measurements from the smallest veins on a linear scale. (B) Vein microstructures in two-dimensional models for different opening apertures (D_m), using a setup with 17.5% transgranular segments. ξ —dimensionless factor of relative growth rate differences between transgranularly versus intergranularly fractured grains. Colors illustrate crystal orientations according to the legend in Figure 2E. (C) Optical photomicrograph under crossed polarizers of a natural wide-blocky vein.



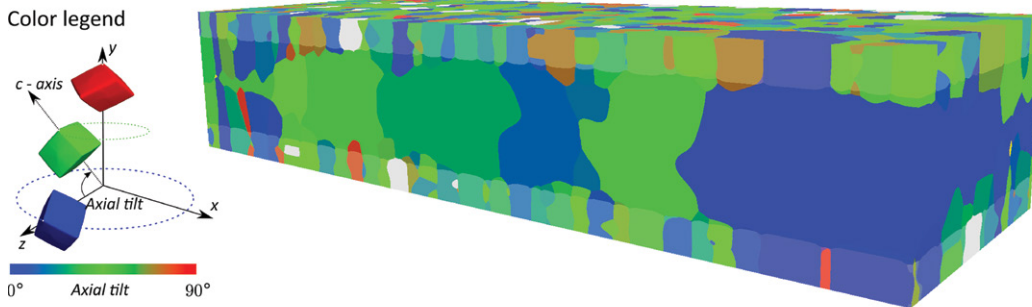
($\xi = 0$), (2) clay-covered intergranular microcracks in calcite with slow growth rates ($\xi = 1$), and (3) clean transgranular microcracks along calcite cleavage planes with fast growth rates ($\xi = 5$ –20). The proportions of these surfaces

were based on measurements along profile lines on an experimental fracture surface (Fig. 2D). Only grains that underwent transgranular fracture are mirrored on both sides of the fracture wall in the model.

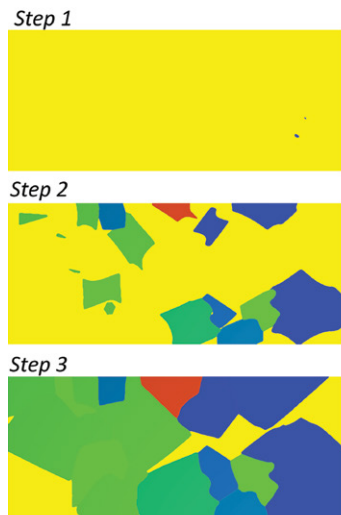
SIMULATION RESULTS

Curves of the W/D_m relationship produced by numerical models show good correspondence with our measurements performed on natural veins (Fig. 3A). Models show that larger initial

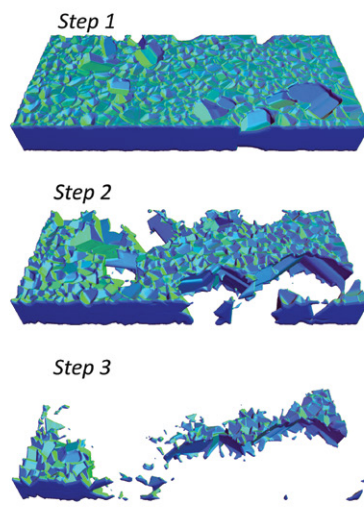
A 3-D model ($D_m = 4$; $\xi = 5$)



B Grains at median line



C Porosity evolution



D Fluid pathways

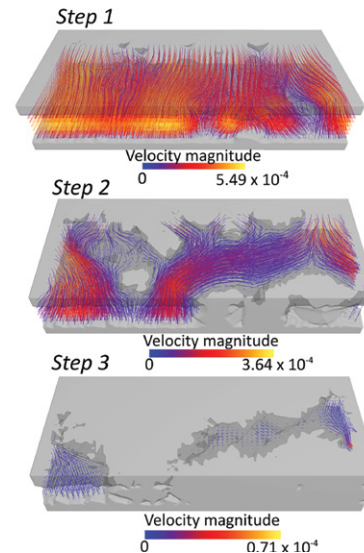


Figure 4. (A) Simulated vein microstructure in three dimensions (3-D). Colors show the orientation of calcite c-axis with respect to the fracture orientation; host rock is shown with faded colors. D_m —vein aperture; ξ —dimensionless factor of relative growth rate differences between transgranularly versus intergranularly fractured grains. Distribution of fast-growing grains is based on the morphology of the experimental fracture (Fig. 2D). (B) Two-dimensional sections across the center of vein showing grains that have reached the median line at three successive stages of vein filling. Yellow marks fluid-filled parts of the vein. (C) Porosity (blue) evolution during fracture filling. (D) Streamlines showing changes in permeability and fluid flow rate during fracture filling. B-D shows a rotated view of A, with the long side perpendicular to the viewer. Velocity magnitude is non-dimensional, expressed as grid spacing (Δx) versus time increment (Δt).

fracture apertures result in wider crystals, but there is a maximum width that vein crystals can reach (plateau) that is dependent on the proportion of “fast-growing” grains in comparison to “slow-growing” and “inert” grains on fracture surfaces. Furthermore, the growth-rate difference (ξ) determines the slope of W/D_m , so that a larger ξ produces wider crystals.

Figure 3B shows that, regardless of fracture aperture, wide-blocky microstructures form only in cases where $\xi > 1$. If $\xi = 1$, the veins consist of blocky crystals with typical growth competition microstructures and a prominent median line. Increasing the initial fracture aperture results in fewer and wider grains at the median line (as in Prajapati et al. [2018]).

In simulations where $\xi > 1$, fast-growing grains on transgranular cleavage planes outgrow slow-growing grains at early stages. However, for low ξ values and small fracture apertures ($D_m < 2$), most slow-growing grains can still reach the other side of the fracture wall, blocking the lateral expansion of the fast-growing grains (Item S3). If the growth rate difference is large ($\xi \sim 20$), slow-growing grains are outcompeted almost immediately, and the width of the wide-blocky grains remains constant regardless of the

initial fracture aperture and/or further changes in ξ (Item S3).

Most of the simulations were performed in 2-D to allow reasonable computational time for setups with a large number of grains. However, 3-D runs are also possible, and we show the results of some such runs in Figure 4. Figures 4B–4D show the evolution of porosity and fluid flow at three stages of vein filling. At early stages (step 1), the fracture is highly permeable and fluid-flow rate is high. As filling progresses (step 2), the two parts of the broken, fast-growing crystals on transgranular fracture surfaces touch near the median plane of the fracture and form bridges, then continue to grow laterally. Fluid pathways and pores remain mostly interconnected until $>50\%$ of the grains have crossed the median line. After that, the porosity structure changes and permeability decreases as pores become isolated (step 3).

DISCUSSION

Our models show that incorporation of differential crystal growth rates for transgranular and intergranular fracture segments is a key for simulating the evolution of wide-blocky veins. We recognize that distinction of only two growth

classes (fast and slow) is a simplification. In natural veins, intergranular fracture segments might have different amounts of clay coatings, or surface defects and transgranular segments might have cleavage steps, both of which affect the precipitation rate of vein minerals. Despite that, our results show a very good correspondence between modeled and natural microstructures, including the quantified trend of increasing crystal width with increasing vein aperture (Fig. 3A) as well as the microstructural characteristics, including distributions of bridge crystals, equidimensional crystals, and rims of small grains along the vein wall (Figs. 1C, 1D, 3B, and 3C).

In addition to the studied location in the UK, wide-blocky vein textures have been documented in micritic limestones from Sestri Levante, Italy (Bons et al., 2012), and the Oman Mountains (Holland and Urai, 2010) but never explained in detail. We infer that wide-blocky textures might be characteristic in clay-rich, micritic host rocks with medium grain-boundary cohesion so that fractures are mostly intergranular, with 25%–5% transgranular segments. However, the heterogeneity of the fracture surface, not the lithology or grain size of the host rock, is the controlling factor in these veins, therefore the observed crystal

growth patterns are likely to operate in a wider range of host rocks that are characterized by composite fracture paths and polymineralic compositions. On the other hand, poorly consolidated rocks with weak grain boundaries that form mostly intergranular fractures are less likely to form wide-blocky veins due to the absence of surface type-dependent crystal growth rate variations. Similarly, wide-blocky textures are not predicted in monomineralic rocks with strong grain boundaries, where most of the fracture is transgranular.

The 3-D models in Figure 4 show how permeability and fluid-flow regime in the wide-blocky veins are strongly affected by the development of crystal bridges early in the filling process. Although these bridges locally block fluid pathways and increase the tortuosity of the flow paths, high pore connectivity is maintained until late stages in the sealing process (Figs. 4B–4D). This is very different from veins where all crystals grow at the same rate and the flow paths are more direct due to the lack of crystal bridges, maintaining higher permeability in the early stages of crystal growth, as was reported by Kling et al. (2017) for quartz veins. However, the early bridge formation in wide-blocky veins might prevent fracture collapse, keeping veins open between fluid pulses.

We infer that once the veins become fully sealed, they are mechanically stronger than the micritic host rock due to the large, bridging crystals that connect both vein walls. Higher mechanical strength implies that new fractures form more easily in the host rock than by a failure of an existing vein. The observed abundance of sub-parallel arrays of microveins rather than larger veins with crack-seal textures suggests that once filled, the studied veins are rarely reactivated.

This study demonstrates the power and versatility of the phase-field method to model the evolution of veins. Its ability to incorporate crystallography, host-rock composition, realistic fracture geometries, differential growth rates, and thermodynamics allows the fine tuning of models to natural vein microstructures.

ACKNOWLEDGMENTS

We thank the German Science Foundation (DFG) for funding this project grants (NE 822/34-1, UR 64/17-1). Ukar acknowledges grant DE-FG02-03ER15430 from the Chemical Sciences, Geosciences, and Biosciences (CSGB) Division, Office of Basic Energy Sciences, U.S. Department of Energy, for financial support, and Sara Elliott for assistance with SEM-CL imaging and post-processing. We thank M. Elburg, S. Cox, Y.D. Kuiper, and an anonymous reviewer for their constructive reviews.

REFERENCES CITED

Ajdkiewicz, J.M., and Larese, R.E., 2012, How clay grain coats inhibit quartz cement and preserve porosity in deeply buried sandstones: Observations and experiments: *American Association of Petroleum Geologists Bulletin*, v. 96, p. 2091–2119, <https://doi.org/10.1306/02211211075>.
Ankit, K., Urai, J.L., and Nestler, B., 2015, Microstructural evolution in bitaxial crack-seal veins:

A phase-field study: *Journal of Geophysical Research: Solid Earth*, v. 120, p. 3096–3118, <https://doi.org/10.1002/2015JB011934>.
Bons, P.D., 2001, Development of crystal morphology during uniaxial growth in a progressively widening vein: I. The numerical model: *Journal of Structural Geology*, v. 23, p. 865–872, [https://doi.org/10.1016/S0191-8141\(00\)00159-0](https://doi.org/10.1016/S0191-8141(00)00159-0).
Bons, P.D., Elburg, M.A., and Gomez-Rivas, E., 2012, A review of the formation of tectonic veins and their microstructures: *Journal of Structural Geology*, v. 43, p. 33–62, <https://doi.org/10.1016/j.jsg.2012.07.005>.
Boullier, A.-M., and Robert, F., 1992, Palaeoseismic events recorded in Archaean gold-quartz vein networks, Val d'Or, Abitibi, Quebec, Canada: *Journal of Structural Geology*, v. 14, p. 161–179, [https://doi.org/10.1016/0191-8141\(92\)90054-Z](https://doi.org/10.1016/0191-8141(92)90054-Z).
Caputo, R., and Hancock, P.L., 1999, Crack-jump mechanism of microvein formation and its implications for stress cyclicity during extension fracturing: *Journal of Geodynamics*, v. 27, p. 45–60, [https://doi.org/10.1016/S0264-3707\(97\)00029-X](https://doi.org/10.1016/S0264-3707(97)00029-X).
Cox, S.F., Etheridge, M.A., and Wall, V.J., 1987, The role of fluids in syntectonic mass transport, and the localization of metamorphic vein-type ore deposits: *Ore Geology Reviews*, v. 2, p. 65–86, [https://doi.org/10.1016/0169-1368\(87\)90024-2](https://doi.org/10.1016/0169-1368(87)90024-2).
Dickson, J.A.D., 1993, Crystal growth diagrams as an aid to interpreting the fabrics of calcite aggregates: *Journal of Sedimentary Petrology*, v. 63, p. 1–17, <https://doi.org/10.1306/d4267a78-2b26-11d7-8648000102c1865d>.
Durney, D.W., and Ramsay, J.G., 1973, Incremental strains measured by syntectonic crystal growth, *in* De Jong, K.A., and Scholten, R., eds., *Gravity and Tectonics*: New York, Wiley, p. 67–96.
Fisher, D.M., and Brantley, S.L., 1992, Models of quartz overgrowth and vein formation: Deformation and episodic fluid flow in an ancient subduction zone: *Journal of Geophysical Research*, v. 97, p. 20,043–20,061, <https://doi.org/10.1029/92jb01582>.
Glen, R.A., Hancock, P.L., and Whittaker, A., 2005, Basin inversion by distributed deformation: The southern margin of the Bristol Channel Basin, England: *Journal of Structural Geology*, v. 27, p. 2113–2134, <https://doi.org/10.1016/j.jsg.2005.08.006>.
Hilgers, C., Koehn, D., Bons, P.D., and Urai, J.L., 2001, Development of crystal morphology during uniaxial growth in a progressively widening vein: II. Numerical simulations of the evolution of antitaxial fibrous veins: *Journal of Structural Geology*, v. 23, p. 873–885, [https://doi.org/10.1016/S0191-8141\(00\)00160-7](https://doi.org/10.1016/S0191-8141(00)00160-7).
Holland, M., and Urai, J.L., 2010, Evolution of anastomosing crack-seal vein networks in limestones: Insight from an exhumed high-pressure cell, Jabal Shams, Oman Mountains: *Journal of Structural Geology*, v. 32, p. 1279–1290, <https://doi.org/10.1016/j.jsg.2009.04.011>.
Kling, T., Schwarz, J.-O., Wendler, F., Enzmann, F., and Blum, P., 2017, Fracture flow due to hydrothermally induced quartz growth: *Advances in Water Resources*, v. 107, p. 93–107, <https://doi.org/10.1016/j.advwatres.2017.06.011>.
Lander, R.H., and Laubach, S.E., 2015, Insights into rates of fracture growth and sealing from a model for quartz cementation in fractured sandstones: *Geological Society of America Bulletin*, v. 127, p. 516–538, <https://doi.org/10.1130/B31092.1>.
Lander, R.H., Larese, R.E., and Bonnell, L.M., 2008, Toward more accurate quartz cement models: The importance of euhedral versus noneuhedral growth rates: *American Association of Petroleum*

Geologists Bulletin, v. 92, p. 1537–1563, <https://doi.org/10.1306/07160808037>.
Laubach, S.E., et al., 2019, The role of chemistry in fracture pattern development and opportunities to advance interpretations of geological materials: *Reviews of Geophysics*, v. 57, p. 1065–1111, <https://doi.org/10.1029/2019RG000671>.
Nelson, R.A., 2001, *Geologic Analysis of Naturally Fractured Reservoirs* (second edition): Boston, Gulf Professional Publishing, 352 p.
Nestler, B., Garcke, H., and Stinner, B., 2005, Multicomponent alloy solidification: Phase-field modeling and simulations: *Physical Review E: Statistical, Nonlinear, and Soft Matter Physics*, v. 71, 041609, <https://doi.org/10.1103/PhysRevE.71.041609>.
Newhouse, W.H., 1942, *Ore Deposits as Related to Structural Features*: Princeton, New Jersey, Princeton University Press, 280 p.
Nixon, C.W., Vaagan, S., Sanderson, D.J., and Gawthorpe, R.L., 2019, Spatial distribution of damage and strain within a normal fault relay at Kilve, U.K.: *Journal of Structural Geology*, v. 118, p. 194–209, <https://doi.org/10.1016/j.jsg.2018.10.016>.
Nollet, S., Urai, J.L., Bons, P.D., and Hilgers, C., 2005, Numerical simulations of polycrystal growth in veins: *Journal of Structural Geology*, v. 27, p. 217–230, <https://doi.org/10.1016/j.jsg.2004.10.003>.
Peacock, D.C.P., and Sanderson, D.J., 2018, Structural analyses and fracture network characterisation: Seven pillars of wisdom: *Earth-Science Reviews*, v. 184, p. 13–28, <https://doi.org/10.1016/j.earscirev.2018.06.006>.
Prajapati, N., Selzer, M., Nestler, B., Busch, B., and Hilgers, C., 2018, Modeling fracture cementation processes in calcite limestone: A phase-field study: *Geothermal Energy*, v. 6, 7, <https://doi.org/10.1186/s40517-018-0093-4>.
Prajapati, N., Abad Gonzalez, A., Selzer, M., Nestler, B., Busch, B., and Hilgers, C., 2020, Quartz cementation in polycrystalline sandstone: Insights from phase-field simulations: *Journal of Geophysical Research: Solid Earth*, v. 125, e2019JB019137, <https://doi.org/10.1029/2019JB019137>.
Ramsay, J.G., 1980, The crack-seal mechanism of rock deformation: *Nature*, v. 284, p. 135–139, <https://doi.org/10.1038/284135a0>.
Schindelin, J., et al., 2012, Fiji: An open-source platform for biological-image analysis: *Nature Methods*, v. 9, p. 676–682, <https://doi.org/10.1038/nmeth.2019>.
Ukar, E., and Laubach, S.E., 2016, Syn- and post-kinematic cement textures in fractured carbonate rocks: Insights from advanced cathodoluminescence imaging: *Tectonophysics*, v. 690, p. 190–205, <https://doi.org/10.1016/j.tecto.2016.05.001>.
Urai, J.L., Williams, P.F., and van Roermund, H.L.M., 1991, Kinematics of crystal growth in syntectonic fibrous veins: *Journal of Structural Geology*, v. 13, p. 823–836, [https://doi.org/10.1016/0191-8141\(91\)90007-6](https://doi.org/10.1016/0191-8141(91)90007-6).
Wendler, F., Okamoto, A., and Blum, P., 2016, Phase-field modeling of epitaxial growth of polycrystalline quartz veins in hydrothermal experiments: *Geofluids*, v. 16, p. 211–230, <https://doi.org/10.1111/gfl.12144>.
Williams, R.T., Farver, J.R., Onasch, C.M., and Winslow, D.F., 2015, An experimental investigation of the role of microfracture surfaces in controlling quartz precipitation rate: Applications to fault zone diagenesis: *Journal of Structural Geology*, v. 74, p. 24–30, <https://doi.org/10.1016/j.jsg.2015.02.011>.

Printed in USA